Published in final edited form as:
Blood. 2013 January 24; 121(4): 595–603. doi:10.1182/blood-2012-07-440339.

Distinct severity of HLH in both human and murine mutants with complete loss of cytotoxic effector PRF1, RAB27A, and STX11

Fernando E. Sepulveda[1,2], **Franck Debeurme**[1,2], **Gaël Ménasché**[1,2], **Mathieu Kurowska**[1,2], **Marjorie Côte**[1,2], **Jana Pachlopnik Schmid**[1,2,3], **Alain Fischer**[1,2,3], **Geneviève de Saint Basile**[1,2,3]

[1]Inserm U768, Paris, France

[2]Université Paris Descartes-Sorbonne Paris Cité, Institut Imagine, Paris, France

[3]Unité d'Immunologie et Hématologie Pédiatrique, Assistance Publique–Hôpitaux de Paris, Hôpital Necker Enfants-Malades, Paris, France

Abstract

Inherited defects of granule-dependent cytotoxicity led to the life-threatening immune disorder hemophagocytic lymphohistiocytosis (HLH), characterized by uncontrolled CD8 T-cell and macrophage activation. In a cohort of HLH patients with genetic abnormalities expected to result in the complete absence of perforin, Rab27a, or syntaxin-11, we found that disease severity as determined by age at HLH onset differed significantly, with a severity gradient from perforin (early onset) > Rab27a > syntaxin-11 (late onset). In parallel, we have generated a syntaxin-11–deficient ($Stx11^{-/-}$) murine model that faithfully reproduced the manifestations of HLH after lymphocytic choriomeningitis virus (LCMV) infection. $Stx11^{-/-}$ murine lymphocytes exhibited a degranulation defect that could be rescued by expression of human syntaxin-11 but not expression of a C-terminal–truncated mutant. Comparison of the characteristics of LCMV infection-induced HLH in the murine counterparts of the 3 human conditions revealed a similar gradient in the phenotypic severity of HLH manifestations. Strikingly, the severity of HLH was not correlated with the LCMV load and not fully with differences in the intensity of cytotoxic activity. The capacity of antigen presentation differed in vivo between Rab27a- and Syntaxin-11–deficient mutants. Our data indicate that cytotoxic effectors may have other immune-regulatory roles in addition to their role in controlling viral replication.

Introduction

The relevance of the immune surveillance performed by cytotoxic T cells (CTLs) is emphasized by immunopathologic disorders that occur when inherited deficiencies impair

Correspondence: Geneviève de Saint Basile, Inserm U768, 149 rue de Sèvres, F-75015 Paris, France; genevieve.de-saint-basile@inserm.fr.

Authorship Contribution: F.E.S. designed and conducted most of the experiments with the assistance of F.D.; G.M. initiated the work; M.K. and M.C. cloned the syntaxin-11 constructs and contributed to genetic data; J.P.S. set up murine experiments for HLH studies; G.d.S.B. supervised the overall project; and G.d.S.B., F.E.S., and A.F. wrote the manuscript.

Conflict-of-interest disclosure: The authors declare no competing financial interests.

The online version of this article contains a data supplement.

Europe PMC Funders Author Manuscripts

the cells' cytotoxic activity. These disorders result in an often fatal condition known as hemophagocytic lymphohistiocytosis (HLH),[1] which is characterized by a nonremitting fever, hepatosplenomegaly, neurologic alterations, hypercytokinemia, expansion and accumulation of activated polyclonal $CD8^+$ T cells, organ infiltration by activated macrophages, and subsequent hemophagocytosis (ie, phagocytosis of blood cells).[2] It is considered that an absence of virus control leads to sustained, polyclonal CTL activation and subsequently excessive macrophage activation.[1,2]

Inherited forms of HLH are caused by mutations in genes for several proteins, including perforin (*PRF1*),[3] Munc13-4 (*UNC13D*),[4] syntaxin-11 (*STX11*),[5] Munc18-2 (*STXBP2*),[6,7] SAP (*SH2D1A*), and XIAP (*XIAP*).[8] HLH may also be associated with hypopigmentation, as in Griscelli syndrome (GS; *RAB27A*)[9] and Chediak-Higashi syndrome (*LYST*).[10,11] In general, HLH-causing mutations affect genes involved in the granule-dependent cytotoxic pathway in CTLs.[12] Syntaxin-11 (STX11) is an atypical SNARE that lacks a carboxy-terminal, hydrophobic, transmembrane domain; instead, it contains a putative palmitoylation motif at the C-terminus that might enable membrane interaction.[13] STX11 deficiency causes familial hemophagocytic lymphohistiocytosis type 4 (FHL4).[5,14]

Murine models of HLH have improved our understanding of the disease mechanism in HLH. Four murine HLH models are available: perforin-deficient ($Prf1^{-/-}$),[15] ashen ($Rab27a^{-/-}$),[16] jinx ($Unc13d^{-/-}$),[17] and souris ($Lyst^{-/-}$).[18] On lymphocytic choriomeningitis virus (LCMV) infection, all 4 models develop most of the HLH features observed in patients. By studying these murine models, we and others have highlighted the pivotal role played by $CD8^+$ T cells and IFN-γ in the development of HLH, the latter being a putative therapeutic target.[15,19]

Here, we describe the generation and characterization of a new murine model of HLH (the $Stx11^{-/-}$ mouse). We show that $Stx11^{-/-}$ mice faithfully recapitulate the key features of human HLH and represent a suitable model for studying FHL4 in vivo and the role of Stx11 in vitro. By comparing the severity of HLH in $Stx11^{-/-}$ mice with that observed in $Rab27a^{-/-}$ and $Prf1^{-/-}$ mice, we established a clear correlation between the murine mutants and the age at HLH onset in their human counterpart. Furthermore, our findings indicate that cytotoxic effectors may have other immune regulatory roles in addition to their role in controlling viral replication.

Methods

Patients

All patients with HLH diagnosis were either previously published or referred for molecular screening (supplemental Tables 1 and 2, available on the *Blood* Web site; see the Supplemental Materials link at the top of the online article). Patients were diagnosed using classic HLH criteria.[2] Written informed consent for genotyping and data collection was obtained from the parents. The study was conducted according to the guidelines of the Declaration of Helsinki. All protocols were approved by the Inserm's institutional review board.

Sequence analysis

DNA samples were prepared from peripheral blood mononuclear cells using standard methods. DNA was used for exon PCR amplification of *PRF1*, *RAB27A*, and *STX11* genes and sequenced (primer sequences available on request).

Mice

Conditional $Stx11^{-/-}$ mutant mouse line was established at the Mouse Clinical Institute–Institut Clinique de la Souris (Illkirch, France). The targeting vector was constructed as follows. A 3.7-kb fragment corresponding to the 3′ homology arm and encompassing exon 2 was amplified by PCR and subcloned in an MCI proprietary vector, resulting in step 1 plasmid. This MCI vector has a floxed neomycin resistance cassette. A 2.4-kb fragment encompassing the floxed exon 3 was amplified by PCR and subcloned in step 1 plasmid to generate step 2 plasmid. Finally, a 4-kb fragment corresponding to the 5′ homology arm was subcloned in the step 2 plasmid to generate the final targeting construct. The linearized construct was electroporated in BD10 (C57BL/6N background) mouse embryonic stem cells. After selection, targeted clones were identified by PCR using external primers and further confirmed by Southern blot with 5′ and 3′ external probes. Positive embryonic stem clones were selected and injected into Balb/CN blastocysts, and male chimaeras derived gave germline transmission. To inactivate the syntaxin-11 gene ubiquitously, *Stx11* fl/fl mice were crossed with C57BL/6 mice carrying the Cre recombinase under the control of the CMV promoter. The transgene was eliminated by genetic segregation. The total excision of neo and exon 3 of *Stx11* was confirmed by analysis of the PCR products. C57BL/6J WT, C57BL/6J-$Prf1^{tm1Sdz}$/J, and C57BL/6J-$Rab27a^{ash}$/J have been described previously.[19] All mice, except Rab27a-deficient mice, were generated on C57BL/6 background. Rab27a-deficient mice were backcrossed to the C57BL/6 background in > 15 generations. Mice were maintained in pathogen-free conditions and handled accordingly to national and institutional guidelines.

Induction of HLH by LCMV infection

The WE strain of LCMV was kindly provided by Professors Maries van de Broek and Rolf Zinkernagel (University of Zürich, Zürich, Switzerland). Mice 6-10 weeks of age received an intraperitoneal injection of 200 pfu of viral particles. Blood counts were checked for several days after infection using an automated cell counter (the MS 9-5 V, Melet Schloesing Laboratories). Serum levels of lactate dehydrogenase and aspartate aminotransferase were determined using the VetTest Chemistry Analyzer (IDEXX Laboratories). The serum IFN-γ concentration was determined using an ELISA kit (eBioscience). The serum levels of other cytokines and chemokine were quantified using multiplex assays (Invitrogen). To quantify CXCL10 production in infected tissues, total RNA was purified using an RNeasy Mini kit (QIAGEN) and cDNA was prepared using the QuantiTect Reverse Transcription kit (QIAGEN). Real-time PCR was performed with a TaqMan Probe Mix (Applied Biosystems) using predesigned primer/probe sets for mouse β-actin (Mm 00607939_s1) and CXCL10 (Mm 00445235_m1; Applied Biosystems).

The quantification of the LCMV load in organs was performed by quantitative PCR, as described previously.[19] Briefly, cDNA was isolated from tissue samples

and analyzed with primers for LCMV (forward: 5′-TCTCATCCCAACCATTTGCA-3′ and reverse: 5′-GGGAAATTTGACAGCACAACAA-3′) and β-actin (forward: 5′-CCAGCAGATGTGGATCAGCA-3′ and reverse: 5′-CTTGCGGTGCACGATGG-3′) using SYBR Green PCR Master Mix (Applied Biosystems).

In vitro CD8$^+$ T-cell activation and degranulation and cytotoxicity assays

Spleen CD8$^+$ T cells were purified from the spleen and activated in vitro with a T-cell activation/expansion kit (Miltenyi) in the presence of 50 U/mL of recombinant IL-2. After 5 days, T-cell degranulation was assayed by activating 4×10^5 cells with different concentrations of anti-CD3e (clone 500A2, eBioscience), in the presence of FITC-coupled anti-CD107a (clone 1D4B, eBioscience) and anti-CD107b (ABL-93, eBioscience) antibodies. Degranulation capacity was assayed in CD8$^+$ T cells supplemented or not with 1000 U/mL of recombinant IL-2 and compared with nonactivated cells and the corresponding isotype control. CD8$^+$ T-cell cytotoxicity was quantified using the CytoTox96 Non-Radioactive Cytotoxicity Assay (Promega). Anti-CD3–loaded P815 cells were used as targets.

CD8$^+$ T-cell transfection

Using a nucleofection kit (AMAXA Biosystems) according to the manufacturer's instructions, 5×10^6 in vitro-activated CD8$^+$ T cells were cotransfected at day 4 with 3 μg of cDNA coding for CFP plus WT human *STX11* or the truncated Y255X mutant. Sixteen hours later, cells were harvested and the degranulation capacity was assayed as described in the previous paragraph.

In vivo T-cell proliferation—To quantify T-cell proliferation, CFSE-labeled P14 CD45.1 CD8 T cells were transferred into control, *Stx11*$^{-/-}$, *Rab27a*$^{-/-}$, and *Prf1*$^{-/-}$ CD45.2 mice previously infected with 200 pfu of LCMV 7 days previously. Three days later, CFSE dilution was assessed by FACS analysis (gated on CD8$^+$ CD45.1$^+$ cells).

In vitro NK cell culture and degranulation assay—NK cells were purified from the spleen (Miltenyi, NK cell isolation kit) and cultured in vitro in the presence of 30 ng/mL of recombinant IL-15. After 6-8 days, NK cell degranulation was assayed by activating 5×10^5 cells with target YAC-1 cells, in the presence of FITC-coupled anti-CD107a (clone 1D4B, eBioscience) and anti-CD107b (ABL-93, eBioscience) antibodies. Degranulation capacity was assessed in NK cells from WT B6 and *Stx11*$^{-/-}$ mice supplemented or not with 1000 U/mL of recombinant IL-2 and compared with nonactivated cells and the corresponding control isotype.

Preparation of macrophages and phagocytosis assay

Bone marrow–derived macrophages were prepared from WT B6 control and *Stx11*$^{-/-}$ mice by culturing precursors for 6 days in M-CSF supplemented medium. Cell differentiation was monitored by FACS analysis.

To determine phagocytic capacity, bone marrow–derived macrophages were mixed for 15 minutes at 37°C with different ratios of Alexa-488–labeled 3-μm NH2-beads (Polyscience).

After the pulse, the total binding plus internalization was analyzed by FACS after resuspending the cells in 20mM citrate buffer, pH 4.0. To specifically quantify the percentage of cells that internalized beads, the cells were resuspended in 0.2 mg/mL of Trypan blue to quench fluorescence of noninternalized particles and analyzed by FACS.

Statistical analysis

Data were analyzed with GraphPad Prism Version 4 software. Survival and HLH incidence curves were analyzed using the log-rank test. All other analyses were performed using *t* tests or 1-way ANOVA with posttest. Differences were considered to be statistically significant when $P < .05$.

Results

Age at HLH onset in FHL2, FHL4, and GS

In humans, the various molecular defects along the cytotoxic pathway that lead to inherited forms of HLH are characterized by similar clinical and biologic manifestations.[1] In all these conditions, both the type of mutation and environmental factors (including virus exposure) can considerably modify the timing of HLH development and the clinical presentation in susceptible patients. Previous genotype/phenotype correlation analyses of perforin deficiency in FHL2 have shown that age at onset is a relevant feature of HLH severity.[20,21] To establish whether deficiencies in perforin, STX11, and RAB27A lead to similarly intense HLH, we compared the age at HLH onset in a large cohort of patients carrying severe biallelic mutations impairing perforin, RAB27A, or STX11 protein expression. Two-thirds of the patients considered were previously reported (supplemental Tables 1 and 2). All the mutations considered are null mutation, introduce a stop codon, or affect the first base of an intron predicted to induce a frameshift and a consecutive stop codon (supplemental Tables 1 and 2). Strikingly, the distribution of ages at HLH onset in patients differed significantly according to the affected gene (Figure 1A-B). Patients lacking STX11, RAB27A, and perforin, respectively, developed HLH at a mean ± SD age of 27.3 ± 37 months, 13.4 ± 19 months, and 3.4 ± 5 months, respectively. Intragroup variance was high for all 3 conditions, emphasizing the role of additive genetic or environmental factors in the development of HLH in humans. In sum, these results indicate a gradient in HLH severity, from perforin deficiency down to STX11 deficiency.

Generation of Stx11-deficient mice

To better characterize the role of STX11 in the immune response, we generated a *Stx11*$^{-/-}$ mouse model. Deletion of exon 3 (the only coding exon in *stx11*) in a C57BL/6 background led to a defect in Stx11 protein expression (Figure 2A). The mice were fertile and grew normally. Compared with *WT* C57BL/6 mice, *Stx11*-deficient mice presented with normal immune cell development and differentiation. Normal counts and proportions of NK, B, T, and antigen-presenting cells were detected in the thymus, lymph nodes, and spleen (data not shown). A normal ratio of $CD8^+$ to $CD4^+$ T cells was observed in the thymus and secondary lymphoid organs (data not shown).

Impaired degranulation of Stx11-deficient murine CTL is complemented by full-length but not a truncated mutant of human STX11

It has been shown that, in FHL4 patients, mutations in *STX11* impair degranulation capacity of cytotoxic lymphocytes and that this defect can be partially restored by incubation with high concentration of recombinant IL-2.[14] To establish whether or not degranulation capacity of murine CTL was dependent on STX11 expression, CD107 cell surface expression was measured in in vitro activated WT and Stx11-deficient murine CTL. As expected, CD107 cell surface expression increased in WT cells after anti-CD3 activation (Figure 2B, left top panel). In contrast, Stx11-deficient CTL failed to degranulate on TCR engagement (Figure 2B, left bottom panel).

To confirm that the degranulation defect observed in Stx11-deficient cells was dependent on Stx11 expression, we carried out complementation experiments by expressing human STX11 in murine Stx11-deficient lymphocytes. Cotransfection of human cDNA encoding STX11 restored degranulation capacity of Stx11-deficient cells to WT levels (Figure 2B-C). Interestingly, expression of a truncated form of STX11 (mimicking a mutation observed in FHL4 patients) did not rescue degranulation capacity of Stx11-deficient cells (Figure 2B-C), even though the mutant was normally expressed (data not shown). As expected, degranulation in WT cells was independent of cell transfection. To determine whether or not activation of murine Stx11-deficient CTL with high concentration of recombinant IL-2 can restore the defect in degranulation capacity, we compared degranulation of WT and Stx11-deficient CTL supplemented or not with 1000 U/mL of IL-2 during the culture. In contrast to human cells, IL-2 was unable to restore degranulation capacity (Figure 2D). Similar results were observed with murine NK cells (supplemental Figure 1). Importantly, the impaired degranulation capacity of Stx11-deficient cells was not related to a defect in CTL activation as expression of activation markers and T-cell proliferation was normal, as shown by expression of CD25 and CD44 and the results of a CFSE dilution assay (Figure 2D-E). Thus, STX11 is absolutely required for the release of lytic granules and requires the C-terminal domain thought to interact with intracellular membranes to function.

Relative severity of HLH in *Stx11*$^{-/-}$, *Rab27a*$^{-/-}$, and *Prf1*$^{-/-}$ mice

To establish whether there are gene-specific differences between the 3 inherited conditions in term of HLH manifestations, a single LCMV-injection (200 pfu) was used to induce and compare the HLH manifestations in *Prf1*$^{-/-}$, *Rab27a*$^{-/-}$, and *Stx11*$^{-/-}$ mouse models. All *Stx11*$^{-/-}$ mice and most of the *Rab27a*$^{-/-}$ mice survived infection in this experimental setting (Figure 3A). As reported previously, *Prf1*$^{-/-}$ mice died ~ 2 weeks after infection with LCMV (Figure 3A). Despite a normal survival rate, *Stx11*$^{-/-}$ mice developed the clinical features of HLH, body weight loss (Figure 3A), a drop in body temperature (Figure 3A), a hunched posture, lethargy, and a general worsening of their condition (as observed in *Rab27a*$^{-/-}$ and *Prf1*$^{-/-}$ mice). The drop in body temperature was significantly less pronounced in *Stx11*$^{-/-}$ mice than in the other 2 murine HLH models (Figure 3A). On day 12 after infection, *Stx11*$^{-/-}$, *Rab27a*$^{-/-}$, and *Prf1*$^{-/-}$ mice presented the typical biologic features of HLH, including pancytopenia (Figure 3B-C) and a lack of neutrophilia (Figure 3D). Increased serum liver transaminase levels were also detected days 8-20 after infection (Figure 3E), together with high serum levels of IFN-γ and inflammatory cytokines,

such as IL-1β, TNF-α and IL-6 (Figure 4A-B). It is noteworthy that the elevation in liver transaminase levels occurred later in *Stx11*$^{-/-}$ mice than in the 2 other HLH murine models (Figure 3E). Serum levels of IFN-γ, known to be a critical factor in the development of HLH, were significantly elevated in all 3 murine models of HLH (Figure 4A). However, IFN-γ levels were lower in *Stx11*$^{-/-}$ mice than in the 2 other HLH models, with *Prf1*$^{-/-}$ mice always displaying the highest levels (Figure 4A).

It has been suggested that CXCL10 expression (an IFN-γ inducible gene) correlates well with the intensity of HLH activity in patients[22] and that CXCL10 could have a role in the recruitment of lymphocytes and macrophages to inflamed tissues. To determine whether this was the case in the HLH murine models, serum levels of CXCL10 were assayed after LCMV infection. An increase in the serum concentration of CXCL10 was observed in all 3 HLH models at day 8 after infection (Figure 4C). The CXCL10 levels correlated well with IFN-γ level (Figure 4D). CXCL10 transcript expression in the spleen was also enhanced (3- to 7-fold vs WT) in all infected mutant mice (Figure 4E). Increased expression of CXCL10 also correlated with splenomegaly, disruption of spleen architecture, and a marked macrophage infiltration (Figure 4F-G).

Overall, LCMV infection induced all the features of HLH in the new *Stx11*$^{-/-}$ mouse. The use of a similar experimental setting to trigger HLH in the 3 murine models revealed a gradient of severity. Based on several phenotypic features (including survival rates, body temperature, serum liver enzyme, and IFN-γ titers), the most intense HLH was observed in *Prf1*$^{-/-}$ mice, followed by *Rab27a*$^{-/-}$ mice and, lastly, *Stx11*$^{-/-}$ mice.

Stx11$^{-/-}$, *Rab27a*$^{-/-}$, and *Prf1*$^{-/-}$ mice have similar viral load

Defective control of LCMV infection is considered to be a key factor in HLH pathogenesis.[15] Hence, viral titers were determined in the spleen and liver of the 3 mouse models at different time points after LCMV infection. Immunocompetent C57BL/6 mice cleared the LCMV in ~ 1 week (Figure 5). In contrast, all 3 cytotoxicity-deficient HLH models failed to control the LCMV infection (Figure 5; and data not shown). Interestingly, the viral load did not significantly differ from one HLH model to another, despite the observed differences in the severity of the HLH manifestations (see previous paragraphs). Thus, although LCMV infection triggers HLH, the viral load does not correlate with disease severity.

Stx11 and Rab27a deficiencies similarly impair cytotoxic activity in vitro

To establish whether the differing HLH severity observed in the 3 HLH murine models correlated with the intensity of cytotoxicity impairment, we assayed the degranulation capacity and/or cytotoxic activity of *Prf1*$^{-/-}$, *Stx11*$^{-/-}$, and *Rab27a*$^{-/-}$ lymphocytes. Compared with WT CTL, *Stx11*$^{-/-}$ and *Rab27a*$^{-/-}$ CD8^{+} T cells failed to degranulate on TCR activation to a similar extent (Figure 6A). The defect in degranulation capacity observed in Stx11- and Rab27a-deficient cells was constant over time and was detected for a broad range of TCR stimulation setting (Figure 6B-C). As expected, normal degranulation capacity was observed in Prf1-deficient CTL compared with control cells (Figure 6A-C). To compare the cytotoxicity defect of the different murine models, in vitro activated CTLs

were incubated with anti-CD3–loaded P815 target cells. Whereas WT CTLs killed target cells efficiently, Stx11- and Rab27a-deficient CTLs showed reduced killing rates to a similar extent, even at high CTL/target cell ratio (Figure 6D). Defect was more pronounced in Prf1-deficient T cells, in accordance with the highest severity of HLH in this model (Figure 6D). Thus, although *Stx11*$^{-/-}$ and *Rab27a*$^{-/-}$ mice exhibit a similar impairment in degranulation and cytotoxicity, the 2 models show difference in HLH severity, suggesting the involvement of additional regulatory mechanism(s).

Contribution of Stx11 and Rab27a to CTL priming

Although one cannot rule out the possibility that in vitro studies do not fully recapitulate cytotoxic function in vivo, mechanisms other than cytotoxicity may also influence the net outcome of the immune response during HLH. It has been shown in in vitro experiments that Rab27a regulates phagosomal maturation and cross-presentation in dendritic cells.[23] Furthermore, in human monocytes, STX11 was reported to be highly expressed, recruited on phagosomes,[24] and restrain phagocytosis of apoptotic bodies.[25] To investigate whether Stx11 plays a role in phagocytic activity of murine macrophages, we generated bone marrow–derived macrophages from control *WT* B6 and *Stx11*$^{-/-}$ mice and phagocytosis of 3-μm latex beads was assessed by FACS analysis. Stx11 deficiency did not impair internalization of latex-bead particles, as Stx11-deficient bone marrow–derived macrophage presented similar phagocytic capacity as control cells (supplemental Figure 2). To determine whether Stx11 and/or Rab27a exert a role in antigen presentation to CD8 T cells in vivo, we transferred CFSE-labeled P14 CD8 T cells to control, *Stx11*$^{-/-}$, *Rab27a*$^{-/-}$, and *Prf1*$^{-/-}$ mice that had been previously infected with LCMV and then measured P14 CD8 T-cell proliferation. Although the 3 murine models displayed similar viral loads (Figure 5), P14 CD8 T cells had a higher proliferative capacity in *Rab27a*$^{-/-}$ mice compared with *Stx11*$^{-/-}$ mice (Figure 7). In contrast, P14 CD8 T-cell proliferation was similar between *Prf1*$^{-/-}$ mice and *Stx11*$^{-/-}$ mice (Figure 7). Even though C57BL/6 mice are able to clear the virus one week after infection (Figure 5), P14 CD8 T cells were still proliferating, a result that is consistent with the persistence of available MHC I–peptide complexes at that time (Figure 7). These data suggest that Rab27a and Stx11 may differently contribute to lymphocyte activation by controlling antigen presentation, thus adding an additional level of complexity in the mechanisms adjusting HLH severity.

Discussion

By comparing the severity of HLH associated with perforin, Rab27a, or syntaxin-11 deficiency, both in humans and in their murine counterparts (including a newly generated *Stx11*$^{-/-}$ mouse), this study brings evidence that effectors of the cytotoxic activity not only control viral infection but also regulate the immune response.

Primary HLH is a genetically heterogeneous disease with a relative homogeneous phenotype.[1] However, considerable differences in the age of disease presentation, severity of clinical symptoms, and duration of remission can be observed. These differences depend on the nature of the molecular causes involved, the type of mutations, potential additional genetic factors, and environmental factors, including virus exposure. We have tried to

restrain some of these factors to better define the effective contribution of 3 different causative defects in the expression of HLH.

In humans, defects in perforin, RAB27A, or STX11 were correlated with the age of HLH presentation. Age of HLH onset was previously shown to be a reliable marker of HLH severity in FHL2 patients.[20,21] To limit the effect of mutation variations, only the patients with biallelic mutations predicting complete loss of protein expression were considered among those previously reported or genetically characterized in the context of this study. Still, a gradient in HLH severity was observed in humans from perforin deficiency down to STX11 deficiency.

The impact of environmental factors and potential additive genetic factors on HLH severity is difficult to appreciate in humans. Thus, animal models of HLH were considered for analyzing the manifestations of HLH in details while controlling these 2 factors. Perforin and Rab27a murine models have been previously engineered or occurred as natural mutant, respectively.[15,16] Here, we generated a syntaxin-11 murine model and, as a first step, evaluated whether or not it recapitulates FHL4 features observed in other HLH murine models.

Stx11$^{-/-}$ mice exhibited a defective degranulation and cytotoxic activity of lymphocytes in vitro, confirming the critical role of this SNARE protein in cytotoxic granule exocytosis. Degranulation defect was complemented by the expression of a full-length human syntaxin-11 protein but not by a protein lacking the last 32 amino acids. The mutant form of STX11 retains the SNARE and the Habc domains, 2 domains thought to interact when SNARE proteins adopt a closed conformation.[26] In contrast, the STX11 mutant lacks the C-terminal domain that contains a putative palmitoylation site thought to mediate membrane association.[13] Membrane localization and switch of the syntaxin-11 protein from a closed to an open conformation are required for SNARE complex formation. This is probably why the truncated form of syntaxin11 is unable to restore lytic granule exocytosis. The *Stx11*$^{-/-}$ mouse should thus be a powerful tool for precisely identifying STX11 regulated steps and the molecular mechanisms involved in CTLs and, potentially, in other immune cells.

As previously shown for perforin- and Rab27a-deficient mice, LCMV infection induced the clinical, biologic, and histologic features of HLH in the new *Stx11*$^{-/-}$ mouse. Although the Stx11-deficient mice survived, they develop characteristic features of HLH, including pancytopenia, elevated serum level of IFN-γ, CXCL10 and inflammatory cytokines, increased levels of liver transaminase, and spleen macrophage infiltration. *Stx11*$^{-/-}$ mouse therefore constitutes a suitable model of FHL4.

A similar experimental setting was then used to compare the manifestations of HLH in the 3 murine models. Remarkably, the intensity of HLH in mice fully paralleled the severity of the disease observed in human HLH patients. *Prf1*$^{-/-}$ mice expressed the most severe manifestations followed by *Rab27a*$^{-/-}$ mice, whereas HLH features in *Stx11*$^{-/-}$ mice were the less intense. Thus, even in controlled environment and genetic background, the same differences in HLH severity, previously observed in humans, were demonstrated in the murine models. This further validates the used of HLH murine models as suitable tools for

studying the mechanism of HLH development in humans. Furthermore, this indicates that the functional consequences associated with each molecular defect significantly differ.

Cytotoxicity defect allowing virus persistence results in T-cell activation and the development of HLH. The 3 cytotoxic-deficient mice failed to clear LCMV infection. However, no difference in the virus load could be detected between them, a finding that could have impacted HLH severity. This suggests that, in addition to a role in virus clearance, the cytotoxic activity of lymphocytes may also contribute to the regulation of immune reactions. Such additional mechanisms may influence the outcome of the immune response by influencing the balance between control of the immune response and a lethal immunopathology. Indeed, the cytotoxic activity may be involved in a “fratricide” mechanism, enabling the immune response to be down-regulated. This hypothesis is further supported by the in vitro observation that, once CTLs have captured membrane fragments from previously killed targets, they themselves can become targets for sister CTLs.[27] Importantly, recent research also suggests that the cytotoxic activity of NK cells plays a direct role in the down-regulation of T cell–dependent viral persistence. A lack of NK cells was indeed shown to increase the proportion of antigen-specific CTLs after LCMV infection[28-30] and hence could facilitate lethal, T cell–mediated diseases. The cytotoxic activity of lymphocytes may thus regulate the outcome of immune responses through a variety of potentially additive mechanisms, allowing a small difference in lymphocyte cytotoxicity in vitro to carry a significant impact in vivo on the regulation of the immune response.

Cytotoxic activity was found severely impaired in all 3 murine models. However, the defect in lymphocytes lacking perforin expression was more pronounced. Through additive cytotoxic-dependent regulatory mechanisms, this subtle in vitro difference may account for the most severe disease expression and lethality observed in vivo in *Prf1*$^{-/-}$ mice. In contrast, the similar cytotoxic impairment observed in *Stx11*$^{-/-}$ and *Rab27a*$^{-/-}$ mice does not correlate with differences in the intensity of HLH manifestations. This suggests that additional regulatory mechanism(s), other than cytotoxicity, may also play a role. Rab27a and syntaxin-11 are broadly expressed, in particular in myeloid cells, and may thus potentially regulate phagocytosis and cross-presentation of antigen. A direct role of these proteins in nonlymphoid cells would add another level of complexity in the mechanisms regulating HLH manifestations. Change in phagosomal function and antigen cross-presentation of Rab27a-deficient dendritic cells has been previously reported in vitro.[23] Interestingly, we observed an increased antigen-specific CD8 T-cell proliferation in vivo when antigen-presenting cells are Rab27a-deficient, supporting a role of Rab27a in antigen presentation. Our work did not allow so far to detect a significant role of syntaxin-11 in antigen presentation, either in vitro or in vivo. Whether or not differences in HLH severity between *Stx11*$^{-/-}$ and *Rab27a*$^{-/-}$ models could be related to differential contributions of these proteins to CTL activation, indirectly via the control of antigen presentation in vivo, will require further studies.

Deciphering the factors that fine-tune the severity of HLH allows to better understand the mechanisms of HLH pathogenesis, in particular, and those regulating the immune response, in general. This should be particularly relevant to approach the pathophysiology

of some types of secondary HLH, which frequently do not express the full picture of HLH. The mouse experiments provide evidence that virus control is a key but not an exclusive variable of LCMV-induced HLH, supporting a direct immune regulatory role of the cytotoxic function of lymphocytes. The HLH murine models are shown here to be reliable counterparts and will be powerful tools to further depict this regulatory mechanism as well as the precise function of these effectors independently of the cytotoxic pathway.

Acknowledgments

The authors thank the clinicians who provided human HLH samples and Nathalie Lambert, Virginie Grandin, Yoan Moreau, and Corina Dragu for their assistance. The mouse mutant line was established at the Mouse Clinical Institute–Institut Clinique de la Souris in the Targeted Mutagenesis and Transgenesis Department with funds from the GIS-Maladies Rares.

This work was supported by the French National Institute of Health and Medical Research (Inserm), the Agence National de la Recherche (ANR Genopath), the Fondation pour la Recherche Médicale, the European Community's FP7 (grant F2-2008-201461), the advanced grant of the European Research Council (PIDImmun, advanced grant 249816), and the Imagine Foundation. F.E.S. was supported by the European Community's FP7 (postdoctoral fellowship) and the Association pour la Recherche sur le Cancer.

References

1. Pachlopnik Schmid J, Cote M, Menager MM, et al. Inherited defects in lymphocyte cytotoxic activity. Immunol Rev. 2010; 235 (1) 10–23. [PubMed: 20536552]
2. Henter JI, Horne A, Arico M, et al. HLH-2004: Diagnostic and therapeutic guidelines for hemophagocytic lymphohistiocytosis. Pediatr Blood Cancer. 2007; 48 (2) 124–131. [PubMed: 16937360]
3. Stepp SE, Dufourcq-Lagelouse R, Le Deist F, et al. Perforin gene defects in familial hemophagocytic lymphohistiocytosis. Science. 1999; 286 (5446) 1957–1959. [PubMed: 10583959]
4. Feldmann J, Callebaut I, Raposo G, et al. Munc13-4 is essential for cytolytic granules fusion and is mutated in a form of familial hemophagocytic lymphohistiocytosis (FHL3). Cell. 2003; 115 (4) 461–473. [PubMed: 14622600]
5. zur Stadt U, Schmidt S, Kasper B, et al. Linkage of familial hemophagocytic lymphohistiocytosis (FHL) type-4 to chromosome 6q24 and identification of mutations in syntaxin 11. Hum Mol Genet. 2005; 14 (6) 827–834. [PubMed: 15703195]
6. Cote M, Menager MM, Burgess A, et al. Munc18-2 deficiency causes familial hemophagocytic lymphohistiocytosis type 5 and impairs cytotoxic granule exocytosis in patient NK cells. J Clin Invest. 2009; 119 (12) 3765–3773. [PubMed: 19884660]
7. zur Stadt U, Rohr J, Seifert W, et al. Familial hemophagocytic lymphohistiocytosis type 5 (FHL-5) is caused by mutations in Munc18-2 and impaired binding to syntaxin 11. Am J Hum Genet. 2009; 85 (4) 482–492. [PubMed: 19804848]
8. Rigaud S, Fondaneche MC, Lambert N, et al. XIAP deficiency in humans causes an X-linked lymphoproliferative syndrome. Nature. 2006; 444 (7115) 110–114. [PubMed: 17080092]
9. Menasche G, Pastural E, Feldmann J, et al. Mutations in RAB27A cause Griscelli syndrome associated with haemophagocytic syndrome. Nat Genet. 2000; 25 (2) 173–176. [PubMed: 10835631]
10. Nagle DL, Karim MA, Woolf EA, et al. Identification and mutation analysis of the complete gene for Chediak-Higashi syndrome. Nat Genet. 1996; 14 (3) 307–311. [PubMed: 8896560]
11. Barbosa MD, Nguyen QA, Tchernev VT, et al. Identification of the homologous beige and Chediak-Higashi syndrome genes. Nature. 1996; 382 (6588) 262–265. [PubMed: 8717042]
12. de Saint Basile G, Menasche G, Fischer A. Molecular mechanisms of biogenesis and exocytosis of cytotoxic granules. Nat Rev Immunol. 2010; 10 (8) 568–579. [PubMed: 20634814]

13. Tang BL, Low DY, Hong W. Syntaxin 11: a member of the syntaxin family without a carboxyl terminal transmembrane domain. Biochem Biophys Res Commun. 1998; 245 (2) 627–632. [PubMed: 9571206]
14. Bryceson YT, Rudd E, Zheng C, et al. Defective cytotoxic lymphocyte degranulation in syntaxin-11 deficient familial hemophagocytic lymphohistiocytosis 4 (FHL4) patients. Blood. 2007; 110 (6) 1906–1915. [PubMed: 17525286]
15. Jordan MB, Hildeman D, Kappler J, Marrack P. An animal model of hemophagocytic lymphohistiocytosis (HLH): CD8+ T cells and interferon gamma are essential for the disorder. Blood. 2004; 104 (3) 735–743. [PubMed: 15069016]
16. Pachlopnik Schmid J, Ho CH, Diana J, et al. A Griscelli syndrome type 2 murine model of hemophagocytic lymphohistiocytosis (HLH). Eur J Immunol. 2008; 38 (11) 3219–3225. [PubMed: 18991284]
17. Crozat K, Hoebe K, Ugolini S, et al. Jinx, an MCMV susceptibility phenotype caused by disruption of Unc13d: a mouse model of type 3 familial hemophagocytic lymphohistiocytosis. J Exp Med. 2007; 204 (4) 853–863. [PubMed: 17420270]
18. Jessen B, Maul-Pavicic A, Ufheil H, et al. Subtle differences in CTL cytotoxicity determine susceptibility to hemophagocytic lymphohistiocytosis in mice and humans with Chediak-Higashi syndrome. Blood. 2011; 118 (17) 4620–4629. [PubMed: 21878672]
19. Pachlopnik Schmid J, Ho CH, Chretien F, et al. Neutralization of IFNgamma defeats haemophagocytosis in LCMV-infected perforin- and Rab27a-deficient mice. EMBO Mol Med. 2009; 1 (2) 112–124. [PubMed: 20049711]
20. Voskoboinik I, Smyth MJ, Trapani JA. Perforin-mediated target-cell death and immune homeostasis. Nat Rev Immunol. 2006; 6 (12) 940–952. [PubMed: 17124515]
21. Feldmann J, Le Deist F, Ouachee-Chardin M, et al. Functional consequences of perforin gene mutations in 22 patients with familial haemophagocytic lymphohistiocytosis. Br J Haematol. 2002; 117 (4) 965–972. [PubMed: 12060139]
22. Takada H, Takahata Y, Nomura A, Ohga S, Mizuno Y, Hara T. Increased serum levels of interferon-gamma-inducible protein 10 and monokine induced by gamma interferon in patients with haemophagocytic lymphohistiocytosis. Clin Exp Immunol. 2003; 133 (3) 448–453. [PubMed: 12930373]
23. Jancic C, Savina A, Wasmeier C, et al. Rab27a regulates phagosomal pH and NADPH oxidase recruitment to dendritic cell phagosomes. Nat Cell Biol. 2007; 9 (4) 367–378. [PubMed: 17351642]
24. Trost M, English L, Lemieux S, Courcelles M, Desjardins M, Thibault P. The phagosomal proteome in interferon-gamma-activated macrophages. Immunity. 2009; 30 (1) 143–154. [PubMed: 19144319]
25. Zhang S, Ma D, Wang X, et al. Syntaxin-11 is expressed in primary human monocytes/macrophages and acts as a negative regulator of mac rophage engulfment of apoptotic cells and IgG-opsonized target cells. Br J Haematol. 2008; 142 (3) 469–479. [PubMed: 18547321]
26. Rizo J, Sudhof TC. Snares and Munc18 in synaptic vesicle fusion. Nat Rev Neurosci. 2002; 3 (8) 641–653. [PubMed: 12154365]
27. Davis DM. Intercellular transfer of cell-surface proteins is common and can affect many stages of an immune response. Nat Rev Immunol. 2007; 7 (3) 238–243. [PubMed: 17290299]
28. Waggoner SN, Cornberg M, Selin LK, Welsh RM. Natural killer cells act as rheostats modulating antiviral T cells. Nature. 2011; 481 (7381) 394–398. [PubMed: 22101430]
29. Biron CA. Yet another role for natural killer cells: cytotoxicity in immune regulation and viral persistence. Proc Natl Acad Sci U S A. 2012; 109 (6) 1814–1815. [PubMed: 22308452]
30. Lang PA, Lang KS, Xu HC, et al. Natural killer cell activation enhances immune pathology and promotes chronic infection by limiting CD8+ T-cell immunity. Proc Natl Acad Sci U S A. 2012; 109 (4) 1210–1215. [PubMed: 22167808]

Europe PMC Funders Author Manuscripts

Key Points

- Syntaxin-11–deficient ($Stx11^{-/-}$) murine model faithfully reproduced the manifestations of HLH after LCMV infection.
- HLH severity differed significantly with a severity gradient from perforin (early onset) Rab27a syntaxin-11 (late onset).

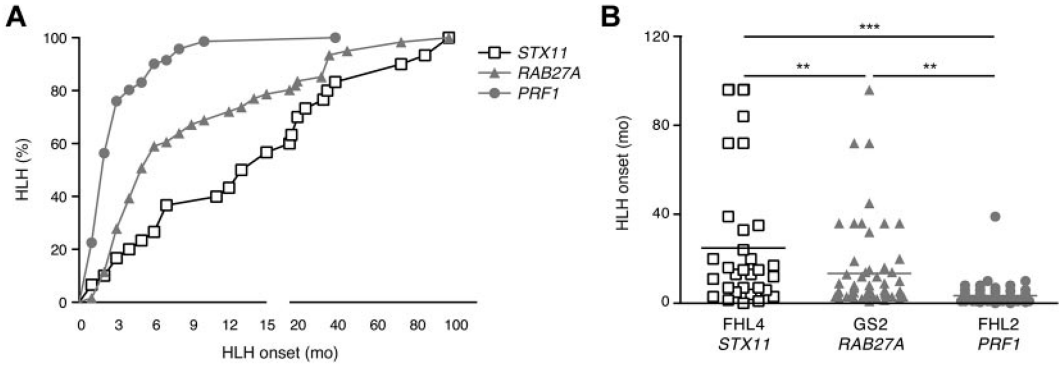

Figure 1. HLH onset occurs later in patients with syntaxin-11 deficiency than in patients with RAB27A- and PRF1$^{-/-}$ deficiencies

(A) Cumulative incidence and (B) age at onset of HLH in FHL2 (PRF1 deficiency, gray circles; n = 72), GS2 (RAB27A deficiency, gray triangles; n = 61), and FHL4 (STX11 deficiency, open squares; n = 30) patients carrying null biallelic mutations, as detailed in supplemental Table 1. The incidence of HLH was analyzed with a log-rank test. *P < .05 for FHL4 versus GS2 patients. ***P < .001 for FHL2 versus GS2 and FHL2 versus FHL4. The onset of HLH was analyzed with a 1-way ANOVA. **P < .01. ***P < .001.

Europe PMC Funders Author Manuscripts

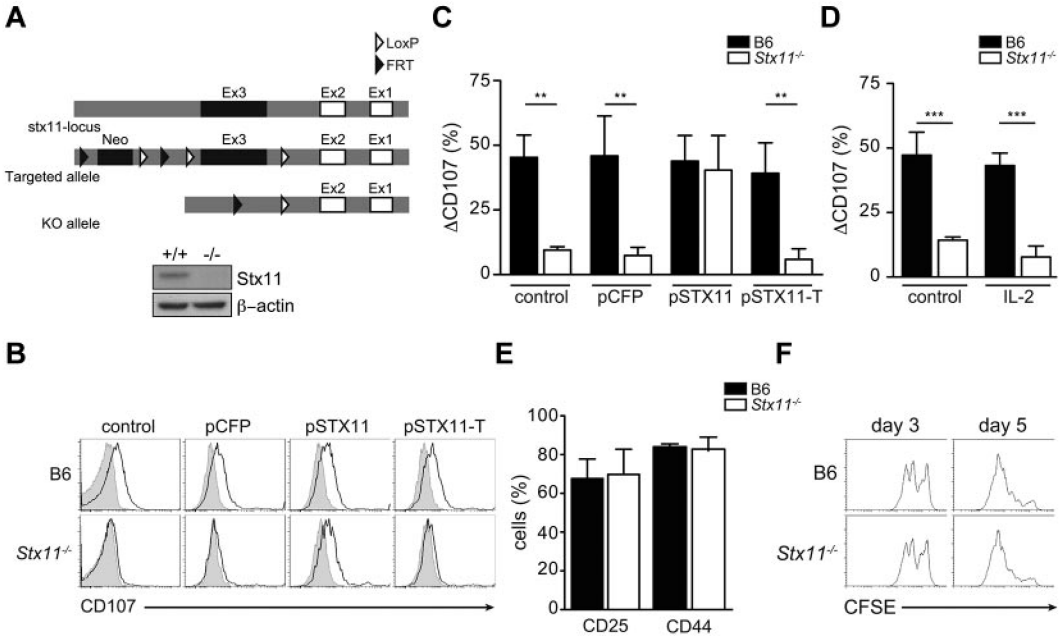

Figure 2. Stx11$^{-/-}$ murine model and complementation of the observed degranulation defect

(A) Top panel: Schematic representation of the approach designed to delete the exon 3 of stx11 in mice. Bottom panel: stx11 (top inset) and β-actin (bottom inset) expression in WT (+/+) and *Stx11*$^{-/-}$ CD8 T cells. (B-F) Spleen CD8 T cells from *Stx11*$^{-/-}$ and control B6 mice were activated in vitro. (B) Control B6 (top row) and *Stx11*$^{-/-}$ (bottom row) CD8 T cells were cotransfected or not (control) with a plasmid coding for CFP (pCFP) alone or together with a plasmid coding for WT STX11 (pSTX11) or a truncated form of STX11 (pSTX11-T). After transfection, degranulation was assessed on stimulation with medium only (filled histogram) or anti-CD3 antibody (black line). (C) Graphs represent the mean ± SEM (n = 4) change in cell surface CD107 on control B6 cells (black bars) and *Stx11*$^{-/-}$ cells (open bars) cotransfected or not (control) with a plasmid coding for CFP alone (pCFP) or together with a plasmid coding for WT STX11 (pSTX11) or a truncated form of STX11 (pSTX11-T). $^{**}P < .001$. (D) Graphs represent mean ± SEM (n = 3) change in cell surface expression of CD107 on control B6 (black bars) and Stx11-deficient cells (white bars) activated in the presence (right panel) or not (left panel) of 1000 U/mL of recombinant IL-2. (E) Graph represents mean ± SEM (n = 6) of percentage of activated CD8 T cells positive for CD25 (left panel) and CD44 (right panel). (F) Representative histograms of CFSE dilution after 3 (left panel) and 5 (right panel) days of culture of control B6 (top row) and Stx11-deficient (bottom row) CD8 T cells.

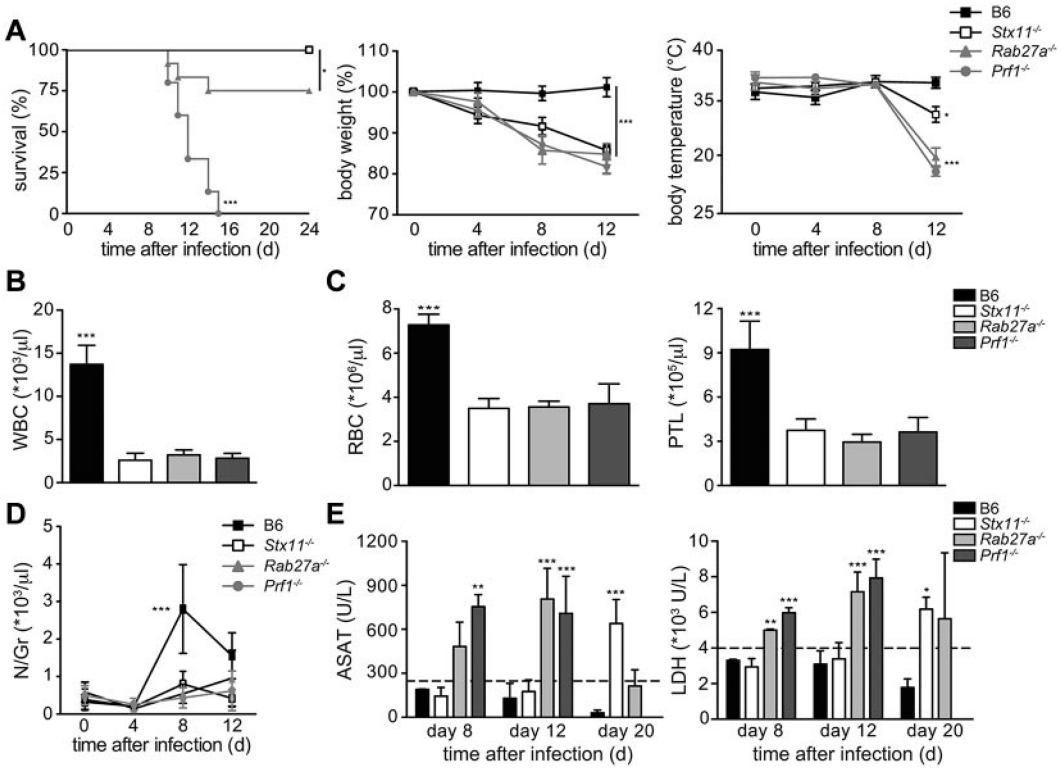

Figure 3. LCMV-infected *Stx11*$^{-/-}$, *Rab27a*$^{-/-}$, and *Prf1*$^{-/-}$ mice display phenotypic manifestations of HLH of variable intensity

Stx11$^{-/-}$ (open bars/open squares), *Rab27a*$^{-/-}$ (light gray bars/gray triangles), *Prf1*$^{-/-}$ (dark gray bars/gray circles), and control B6 (black bars/black squares) mice were infected with 200 pfu of LCMV-WE. Clinical and biochemical parameters were determined after infection. (A) Survival, body weight, and body temperature. Survival was analyzed with a log-rank test (n = 12-16). *$P < .05$. ***$P < .001$. (B) White blood cell counts. ***$P < .001$. (C) Red blood cell and platelets counts. ***$P < .001$. (D) The time course of neutrophil counts. ***$P < .001$. (E) Serum aspartate aminotransferase (ASAT) and LDH levels in infected mice were analyzed on days 8, 12, and 20 after infection. **$P < .01$. ***$P < .001$. Data (mean ± SD) are representative of 4 independent experiments with at least 3 mice in each group.

Europe PMC Funders Author Manuscripts

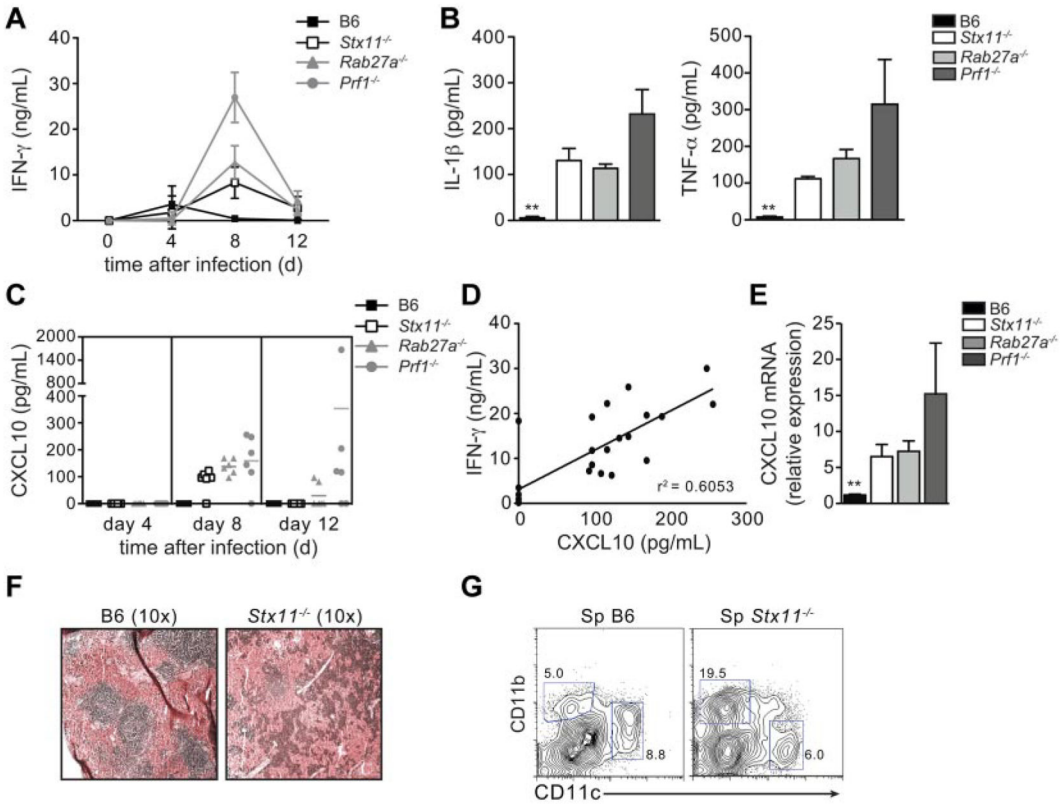

Figure 4. Different levels of inflammatory cytokines are detected in LCMV-infected *Stx11*$^{-/-}$, *Rab27a*$^{-/-}$, and *Prf1*$^{-/-}$ mice

Stx11$^{-/-}$ (open bars/open squares), *Rab27a*$^{-/-}$ (light gray bars/gray triangles), *Prf1*$^{-/-}$ (dark gray bars/gray circles), and control B6 (black bars/black squares) mice were infected with 200 pfu of LCMV-WE. (A) The time course of serum IFN-γ production. ***$P < .001$ for control B6 versus *Stx11*$^{-/-}$ and *Rab27a*$^{-/-}$ versus *Prf1*$^{-/-}$ at day 8. ***$P < .001$ for *Stx11*$^{-/-}$ versus *Rab27a*$^{-/-}$ and *Stx11*$^{-/-}$ versus *Prf1*$^{-/-}$ at day 8. ***$P < .001$ for *Rab27a*$^{-/-}$ versus *Prf1*$^{-/-}$ at day 8. (B) Serum IL-1β (left panel) and TNF-α levels (right panel) on day 12 after infection. (C) The time course of serum CXCL10 production. (D) Correlation between serum levels of IFN-γ and CXCL10 on day 8 after infection. (E) CXCL10 mRNA in spleen of infected mice. **$P < .001$. (F) Hematoxylin and eosin staining of representative spleen sections of control B6 (left panel) and STX11$^{-/-}$ (right panel) mice 3 weeks after LCMV infection. (G) FACS analysis of spleen cells from control B6 (left panel) and *Stx11*$^{-/-}$ (right panel) mice 3 weeks after LCMV infection, gated on I-Ab+ cells. Data (mean ± SEM) are representative of 3 independent experiments with at least 3 mice in each group.

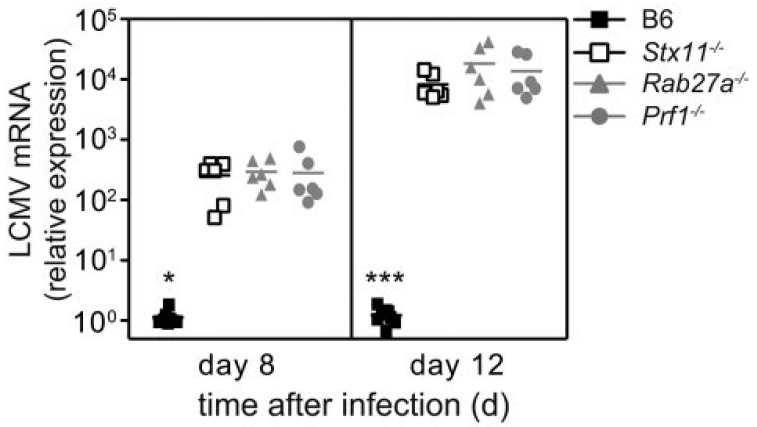

Figure 5. Defective control of LCMV infection in *Stx11*$^{-/-}$, *Rab27a*$^{-/-}$, and *Prf1*$^{-/-}$ mice

Stx11$^{-/-}$ (open squares), *Rab27a*$^{-/-}$ (gray triangles), *Prf1*$^{-/-}$ (gray circles), and control B6 (black squares) mice were infected with 200 pfu of LCMVWE. After 8 or 12 days after infection, LCMV titers in the spleen were determined. Data (mean ± SEM) are representative of 3 independent experiments with at least 3 mice in each group. *$P < .05$. ***$P < .001$.

Europe PMC Funders Author Manuscripts

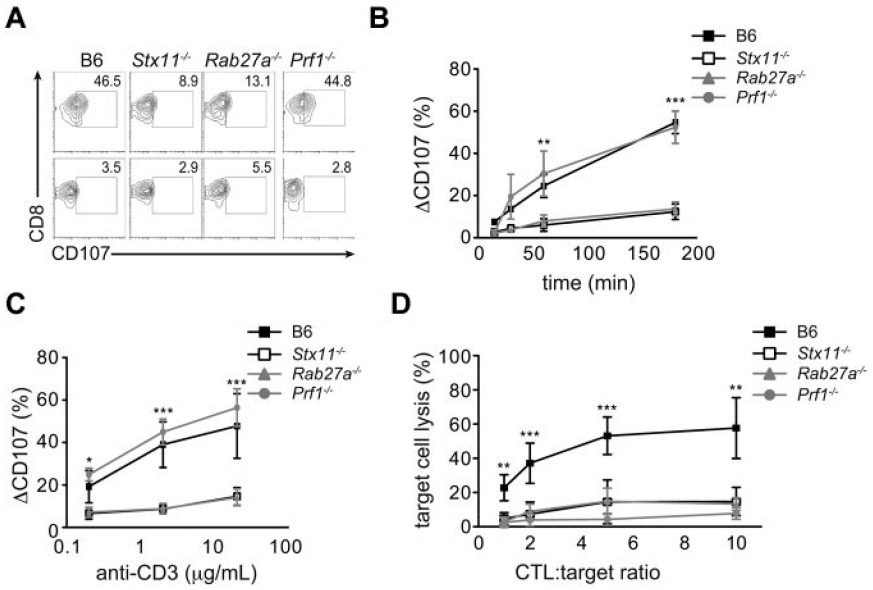

Figure 6. Intensity of CTL degranulation capacity and cytotoxicity in *Stx11*$^{-/-}$, *Rab27a*$^{-/-}$, and *Prf1*$^{-/-}$ mice

Spleen CD8 T cells from *Stx11*$^{-/-}$, *Rab27a*$^{-/-}$, *Prf1*$^{-/-}$, and control B6 mice were activated in vitro. (A) A representative FACS analysis for degranulation of CD8 T cells from control B6 (left panel), *Stx11*$^{-/-}$ (left middle panel), *Rab27a*$^{-/-}$ (right middle panel), and *Prf1*$^{-/-}$ mice (right panel) on stimulation with medium (bottom row) or anti-CD3 antibody (top row). (B-C) Graphs show the mean ± SEM (n = 5) CD107 variation on control B6 (black squares), *Stx11*$^{-/-}$ (open squares), *Rab27a*$^{-/-}$ (gray triangles), and *Prf1*$^{-/-}$ (gray circles) CD8 T cells after anti-CD3 stimulation over time (B) or with different concentrations of anti-CD3 antibody (C). **P* < .05. ***P* < .01. ****P* < .001. (D) Cytotoxicity was determined in activated CD8 T cells after incubation with target anti-CD3–loaded P815 cells for 3 hours. Data (mean ± SEM) are representative of 3 independent experiments performed in triplicate. **P* < .05. ***P* < .01. ****P* < .001.

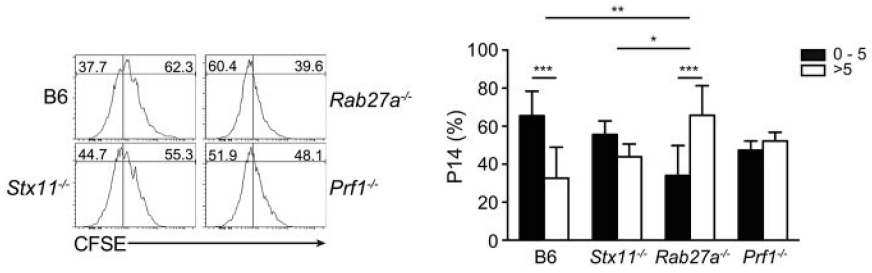

Figure 7. Increased cross-presentation in *Rab27a*$^{-/-}$ mice in vivo

CFSE-labeled P14 CD8 T cells were transferred to LCMV-infected control B6, *Stx11*$^{-/-}$, *Rab27a*$^{-/-}$, and *Prf1*$^{-/-}$ mice. The figure shows representative histograms of CFSE staining in P14 cells 3 days after transfer (right panel) and the proportion of P14 cells having divided between 0 and 5 times (black bars) or more than 5 times (white bars). Graphs represent the mean ± SD value from 2 independent experiments with 3 mice in each group. *$P < .05$. **$P < .01$. ***$P < .001$.

Europe PMC Funders Author Manuscripts